External perturbations and structure of the β Pictoris disc

Anders K. Jeneskog

April 26, 2001

Abstract

The main sequence star β Pictoris which was once considered ordinary, now intrigues astronomers because of its large and asymmetrical circumstellar disc. The disc was discovered because its dust radiated in infrared but it is in fact detectable in a broader spectrum. There are some large scale asymmetries, as well as an inner warping peaking at 70 AU from the star. There are also claims of an observed ring structure in the dust disc.

I have addressed the issue of structure formation in a dust disc surrounding a star with numerical dynamical simulations of the external perturbation of the disc by a stellar flyby. The simulations have been done on the parallel computer Hydra using MPI (Message Passing Interface) for sharing information between its 8 nodes.

Simulating a star passing a planetesimal disc on a parabolic trajectory generates a ring structure, consisting of several spirals in the disc; however, this is not the case if a dust disc is simulated. The key difference between planetesimal and dust dynamics is the additional radiation pressure.

Simulating a long period binary, a perturber on a elliptic orbit, passing a planetesimal disc first generates a similar ring structure as for a parabolic encounter, but as the binary returns the structures are destroyed. And field stars simulated on hyperbolic trajectories pass too quickly to produce any of the desired structures.

The large scale asymmetries of β Pictoris could possibly be explained by a flyby, but the difficulties in generating both the inner warp and the outer regular ring structure support the idea of a planet as a perturber.

Contents

1 Introduction

The Sun was born out of a cold gas cloud collapsing under its own gravity rotating faster and faster and flattening out to a disc, the central part forming the Sun and the rest of the disc spawning the planets. This idea is indeed an old one, clearly postulated by Immanuel Kant in 1755 [19]. This introduction will try to give a modern account to these events.

1.1 Protostar formation

The collapsing cloud was a part of what now is known as the interstellar medium. Its composition and other properties are of importance for the study of stellar and planet formation.

Its chemical composition is over all in accordance with the cosmic abundance, that is 74% hydrogen, 25% helium and 1% metals. Dust grains are also found in the interstellar medium. The effects of dust are seen in dark nebulae and reflection nebulae. The dark nebulae have a higher density of dust than reflection nebulae and therefore a higher opacity, generally the dust scatters and absorb much more efficiently than gas clouds do. The temperature of a dark nebula is about 10K to 10^2K and molecules can form.

Stars form out of the interstellar medium when the density is sufficiently high and temperature low enough to make the gravity overcome the gas pressure. In dark nebulae this is the case.

But something is needed to trigger the event, for example the collision of two interstellar clouds, a nearby supernova explosion or the passage of clouds through a spiral arm of the galaxy. The volume number density is about a 1000 times higher in these kinds of objects than in the interstellar medium, which have a density of about 1 particle per cm^3.

As the nebula starts to contract gravitational energy is converted into heat. This phenomenon is called the Kelvin-Helmholtz contraction. At start the energy escapes the nebula because it is optically thin. But at a certain state it turns thick and the heat generated is transported out of the primordial nebula by convection. This is however a slow process and the nebula starts to heat up and after a few thousand years the surface reaches a temperature of 2000K to 3000K.

The formula $L = 4\pi R^2 \sigma T^4$ shows why a protostar in its early age is very bright due to its large radius R. At some point in time the nebula will come to a hydrostatic equilibrium, and it is recognized as a stellar object. Some protostars eject mass into space due to strong magnetic fields at their surface. This is the T-Tauri phase of the protostar and it starts at the age of 10^6 years and lasts for approximately 10^7 years.

The average rate of mass loss is 10^{-8} to 10^{-7} solar mass a year, this the T Tauri wind. And as energy is lost into space the contraction can continue.

Another interesting feature of T Tauri stars is that their luminosity can change over a few days. This is unexplained but three reasons are proposed. First, that dark clouds in the nebulae pass in front of the star blocking path of light. Second, that a strong magnetic field creates nonlinear flows of matter on to the star which changes the luminosity. In a way this can be viewed as the same process as sun spot and solar eruptions but with a matter flow in the opposite direction. And third the possibility of a undetectable companion, either a plant or a binary star which could cause the irregular patterns of luminosity.[20]

Pre-main sequence stars are classified according to weight. T Tauri stars are low mass stars and they have a mass less than 3 solar masses, stars more massive do not vary in their luminosity, but they also lose mass due to the strong radiation pressure at their surfaces. The intermediate weight class of these youthful stars are called Herbig Ae/Be stars and has a typical weight which is less than 8 solar masses. [22] Herbig Ae/Be may have spherical envelopes and not discs. Herbig Ae star present emission lines which are shining from inside the interstellar cloud in which they have formed. The process of magnetically funneled accretion which results in hot spots on T Tauri stars is not found on Herbig Ae/Be stars, nor are there any large cool spots on the surfaces of these stars.

Young stars can also lose mass by a so called bipolar outflow which consists of two diametrically opposed jets. The gas ejected collides with surrounding interstellar medium and forms to regions of ionized gas that have emission line spectra. These objects are known as Herbig-Haro objects. They exist under a short period of time 10^4 to 10^5 years and through this process more than half of the star's original mass is ejected.

The λ Boötis stars are population I A-type star [13] which are under abundant of metals and many are young, about zero age main sequence stars. The low metal abundance in photosphere because dust free interstellar gas is accreting on the star while dust is being repelled by the radiation pressure from the star. Some λ Boötis stars show evidence of circumstellar material, either in the form of dust, or shell absorption.

1.2 Protoplanetary discs

Many stars have massive and optically thick accretion discs especially stars with bipolar outflow. Observationally these discs have masses ranging from 0.01 to 0.1 solar masses. And in some of these accretion discs and primordial nebulae planets are expected to be formed, these are called protoplantary discs.

The protostar both eject and accrete mass as the nebula contracts. The governing principle is the conservation of angular momentum and as the nebula contracts it spins faster and by spinning it flattens out. Examine the schematic description in Figure 1.

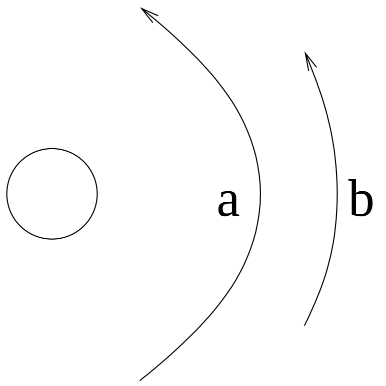

Figure 1: Schematic picture of the solar nebula showing elements in the disc on Keplerian orbits.

Initially one can see the disc as consisting of element on Keplerian orbits, at (a) higher velocity closer to the star than (b). But because the disc is more like a fluid disc there is friction in it. This tends to make the disc more like a rigid body and as particles of greater radius vector (b) increase their speed implies an increased angular momentum $\vec{l} = \vec{r} \times \vec{v}$ they spiral out from the protostar, the particles of shorter radius vector (a) on the other hand lose speed and angular momentum and spirals into the star. The nebula has turned from a spherical object to a more disc-like one which becomes more and more thin. Angular momentum has been transported out from the star, allowing for the matter to travel in towards the star.

If collision is the only cause of friction it will take more time to redistribute mass in the nebula than the age of the solar system. There are many models to explain the viscous stress, they might cooperate or some may be completely invalid. The most important and preferred model today is the magneto-rotational instability model, though it originally dates back to Chandrasekhar it was rediscovered by S. A. Balbus and J. F. Hawley. Here follows a summary of the rigorously understood convection model.

In the nebula the temperature is below 2000K and dust grains can form. The opacity due to the dust grains goes roughly with the square of the temperature. So when the nebula is optically thick it cools off slowly as it takes the radiation long time to leave. On the other hand if the nebula has a low temperature it has low opacity and therefore cools off faster. This provides the temperature of the nebula with a strong conservative feedback mechanism. This stratifies the nebula vertically with respect to temperature, pressure and opacity and this vertical structure of nebula comes into hydrostatic equilibrium. Gravity and gas pressure is balanced. However the nebula is never completely homogeneous due to many unforeseen stochastic processes. Consider a small hot element of the nebula. Hot means hotter with respect to it surrounding, then it will rise upward by buoyancy effect. And doing so it will expand. Until it reaches a new equilibrium. As the element is now less dense it is also optically thinner and it will lose some of its energy by radiating it out into space. The temperature becomes lower and as the element becomes denser again it will sink. This is convection. For a general treatment of convection in fluids see [23].

Also, if the nebula has a high temperature, that is, close to the star where the dust grains are vaporized, it also has a high opacity which is accounted for by the vaporized molecular transition and negative hydrogen ions. And this leads again to convection.

But convection does not only solve the problem of redistributing angular momentum as the convective cells transport matter with higher angular momentum outwards from the star, but it also provides a method for the production of heat as the convection is a multiscale turbulence which begins with a kinetic form of energy and ends in heat. Finally, the convective process transfer heat from the inner parts of the nebula to the outer parts.

1.3 Evolution toward gas-free disks

During infalling stage matter falls in to the nebulae faster than redistribution of matter. And this leads to a buildup during a period of $6\times10^4 - 10^6$ years. There are at least two reasons that could lead to its end. First, because material in the cloud in which the star was formed has come to an end. And second, the viscous diffusion rate equals the rate of matter redistribution. [8] This process is the accretion.

When the accretion comes to an end a viscous stage takes place and the nebula's mass decrease and the protostar's mass increase until a new equilibrium can be reached, the so called minimum mass nebula. This takes $10^5 - 10^6$ years. The structure obtained can roughly be split into three regions. Closest to the star there is the dissociation and ionization region where the temperature is $10^4 - 2\times10^5$K and it radiates in optical and ultraviolet wavelengths. Beyond this region is the metal grain region where the temperature has dropped below 2000K and grains of metal can form which radiates in extreme, far and near infrared wavelengths. In the outer region of the nebula, the so called ice grain region, temperature drops below 160K and it will radiate in extreme and far infrared wave lengths.

After the state of the minimum mass nebula is reached, gas and fine dust is removed in what is called the clearing stage and the disc is transformed from a optically thick to optically thin object. There are at least two models which are primarily used to explain this, first a strong stellar wind or photoevaporation. As mentioned above the stellar wind from T Tauri stars are most often perpendicular to the plane of the accretion disc, this makes the process inefficient. Second, the interaction of protoplanets and nebular gas can achieve a clearing of nebular material by open gaps in the disc in the orbits of planets. Then a gap opens the planet inside can continue to grow due to a flow of matter through the gap which ultimately helps to deplete the disc from matter.[4] Depending on what theory and initial conditions used this clearing stage continues for a few thousands to a few million years.

As the protoplanetary disc clears out the most gas some dust will remain even though its total mass will decrease. This is confirmed by the fact that most stars of age $\sim 0.3 \times 10^6$ years have optically thick discs close by, but only a few percent at the age of10^7 years. [25]

1.4 Vega-type systems

IRAS, InfraRed Astronomical Satellite, started its measurements in 1983. Vega among other stars distinguish themself by their larger flux of infrared radiation in comparison with that the photosphere could supply. Vega or α Lyrae an A0V star at a distance of 8.1 pc was the first star of this kind therefore it gave its name to the group. The infrared excess was quickly understood as the thermal radiation from solid grains around the star, that is, a warm circumstellar dust disc which in this case dominates over the photospheric flux from the star. [2]

The Vega-type stars can be split in two subgroups one with little dust (gas-poor) and much dust (gas-rich).

Later studies have concluded that about 20% of the main sequence stars of type B, A and F have an infrared excess, and presumably therefore has circumstellar discs. The corresponding number for G-type stars are 50%. These numbers may be an slight over estimate. But in a few cases, β Pictoris, 55 Cancri, HR4796A and HD 141569 the star light scattered of the warm circumstellar disc has been imaged by coronographs. [2] See also Figure 2.

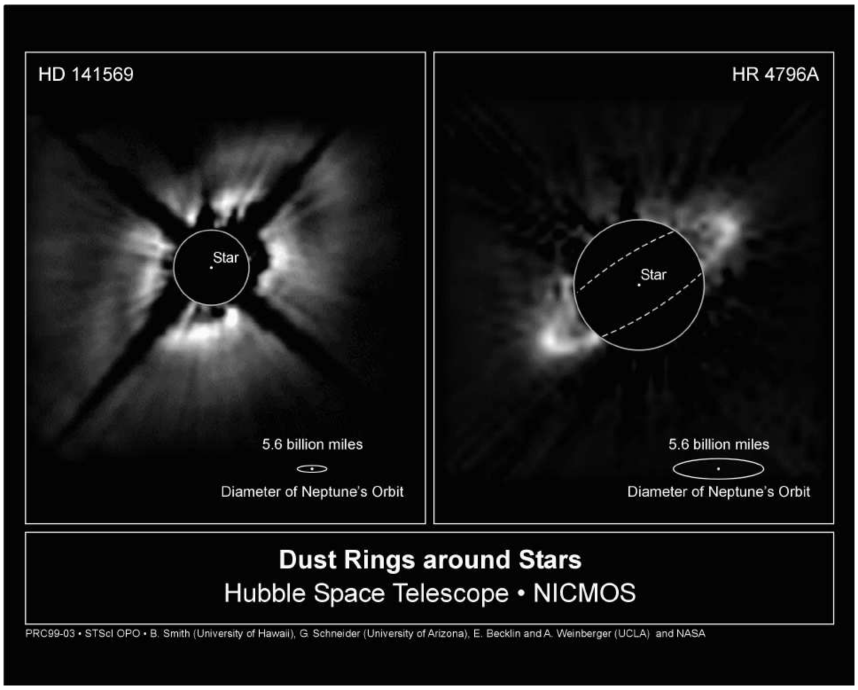

Figure 2: Dust discs of two 10^7 year old stars HR 4796A and HD 141569 imaged with NICMOS.

1.5 Kuiper belt and zodiacal light

In the solar system there are two main reminents of the protoplanetary disc from which the planets formed that is the Kuiper belt and the zodiacal light.

The Kuiper belt, also known as the Edgeworth-Kuiper belt, consists of large number of bodies in transneptunian orbits roughly in the ecliptic plane. These bodies can be described as planetesimals. The Kuiper belt was introduced as an idea to explain the source of the short period comets, who in contrast to long period comets are assumed to originate from the so called Oort cloud.

$$n(r)dr = \Gamma r^{-q} \tag{1}$$

From equation (1) there $\Gamma = 3.8 \times 10^{10}$ and $q \sim 4$ we have that there are approximately 10^5 Kuiper belt objects larger than 50km. That there should be 10 Pluto-scale object, that is larger than 1000km and 10^{10} objects larger that 1km.

The 30-AU to 50-AU region is the classical Kuiper belt region. Due to Neptune the region outside 42 AU should be more densely populated. But with a finite mass and with a surface mass density (e.g. R^{-2}) the disc must have an outer limit. And all known Kupier belt object are found with a semi-major axis in between 35AU to a 115AU. [15]

Inside the solar system there exist a very thin disc or cloud called the zodiacal light disc, which consist of small particles and dust. It is replenished by passing comets and asteroid. The zodiacal light disc probably joins a dusty component of the Kuiper belt, and also probably replenished from the Kuiper belt, possibly measurable. The dust production rate in the Kuiper belt is estimated to be in the interval $10^2 kgs^{-1}$ to $10^7 kgs^{-1}$ and in the zodiacal light disc $10^4 kgs^{-1}$.[15] In comparison with ϵ Eridani and Formhault the zodiacal light disc is 10^2 to 10^4 times less dusty. [4]

2 Beta Pictoris

2.1 The Star

β Pictoris is found on the southern hemisphere, with $\alpha\,(2000) = 05h\,47m\,17.1s$ and $\delta\,(2000) = -51^\circ\,03'\,59''$. The star is located in the Local Bubble, which got its name due to the fact that it is a rather empty region of space. [26] Hipparcos measured that β Pictoris is located 19.28 pc away. It is a normal main sequence star of spectral type A5V, which has a surface temperature of about 8200 ± 100 K. Due to that it is rapidly rotating around its own axis the Doppler shift caused by possible planets is blurred together with the rotational Doppler shift.

2.2 Circumstellar disc

The most prominent star in the group of Vega-type stars is β Pictoris. The infrared excess begins at $12\mu m$ and peaks at $60\mu m$. The temperature of the dust disc the infrared excess tells about is around β Pictoris is about 100K. [1]

The mass of the planetesimals of the disc is approximately 0.5% of total disc mass $(0.05 - 0.1)M_{\odot}$ that is $\sim (120 \pm 40)M_{\oplus}$ The circumstellar dust disc have confirmed dust in the range $6\mu m - 4mm$. Using the standard $dN{\sim}b^{-3.5}\,db$ distribution of size the it confirms a $0.5M_{oplus}$. Extending this up to the mass derived from the primordial nebula gives sizes up to 1km. This would mean that there are no planets, but this oversimplified calculation obviously leave something in precision missing.

β Pictoris is a prototype stars in the group of gas-poor stars, but there are both and gas and plasma present, i.e. the disc is not a proto-planetary disc, but it is in a later stage. A stage there if planets could form they already have.

The edge on view of β Pictoris improves observability and the first coronographic image was made by Smith and Terrile in 1984. [26] Now a paper is under preparation repeating James Keeler's famous confirmation of the rotation of Saturn's ring, though this time for the circumstellar disc of β Pictoris.[7]

The dust disc of β Pictoris has a more gradual density fall-off and extends at least 1000 AU it will not easily be modeled with sharp outer edges, as Vega, Formalhaut (α Piscis Austrinis an A3V star at distance of 15 pc) or ϵ Eridani (a K5V star 3.3 pc away). These stars are due to historical reason from the IRAS the prototypes for the Vega-type systems. [10] There is also observations confirming that the disc has a inner gap of radius $\sim$ 20 AU which is not entirely empty.

The composition of β Pictoris disc is mostly chondritic. Though most C and O are in gaseous form of CO. Free oxygen atoms binds to Si, Mg, Fe and forms silicate grains, this happens in inner nebula then temperature is below 1400-1700K.

Above 500K the olivine, forsterite (Mg_2SiO_4) and the pyroxene, enstatite ($MgSiO_3$) are the most important abundant material. Below 500K iron atoms can also bind so the olivine, fayalite (Fe_2SiO_4) and the pyroxene, ferrosilite ($FeSiO_3$) appears among the most important abundant material. Alas magnesium is more abundant and the ratio is Fe:(Fe+Mg) as 1:5. In the outer part of nebula ($r > 20$ AU, that is, all of the now remaining disc) ices are mixed in, this ice consists of 90% H_2O. [9]

The age of β Pictoris can be but in an interval in between $10 - 100 \times 10^6$ years. Due to its stellar luminosity it shall be older than 10^7 years, and according to the state of circumstellar disc it will be $\leq 10^8$ years.

2.3 Disc asymmetries

Using Space Telescope Imaging Spectrograph (STIS) a coronagraphic visible-light image (Figure 3) was made showing a 3-degree warp of the inner part of β Pictoris disc, this is known as the Butterfly asymmetry. The inner part of the disc ($r \leq 120$ AU) differs from the outer part of the disc not only because of the warp but also because of its much flatter flux distribution. The warp peaks at a 70 AU were it has its maximum vertical displacement (± 1.5 AU). [14] [5]

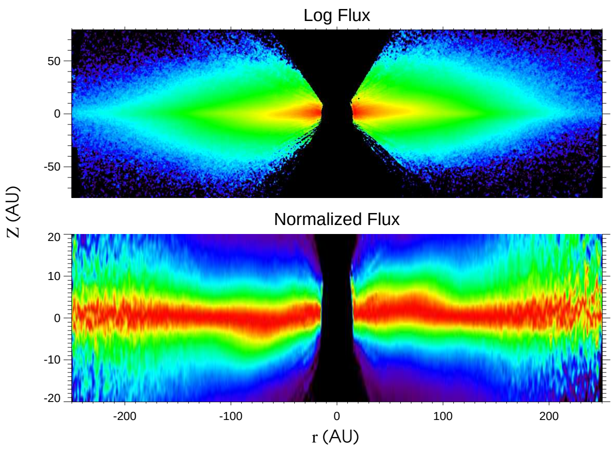

Figure 3: The higher panel is the HST/STIS image of β Pictoris made by Heap et al. [14] and the lower panel show the same image processed with the Z-axis rescaled to enable a clearer view of the inner warp.

But there are also other asymmetries. First there is the size asymmetry, the north-east wing is detected out to a projected radius of 48″, while the south-west wing only reaches 40″. Second, the south-west branch is 20% less bright than the north-east wing, this is the brightness asymmetry. Actually the magnitude of the brightness asymmetry increases with radius. Third, the wings of the disc flares at an radius of 7″. However beginning at 9″ the south-west wing flares more then the north-east wing this is the width asymmetry.

And last there is the wing-tilt asymmetry. The position angle of north-east midplane differs from the position angle of the south-west midplane by $\sim 1.3°$. [17] This can however be explained by the fact that the disc is tilted towards earth and that the radiation is reflected by an asymmetrical phase function. [26]

There are several way of explaining the warp of the disc. First, it could form in the pre-main sequence star phase due to radiation-induced instabilities, this is however excluded because the warp when would be asymmetrical, but both sides are equally thick. Second, a planet on a slightly inclined orbit would be able to generate the warp.[26] From the STIS image it is possible to deduce some constraint on the possible planet's properties. Depending upon the age of the β Pictoris system among other. The orbital sizes ranging from 3 AU to 50 AU and the mass ranges from 17.4 M_J to 0.17 M_J. [14]

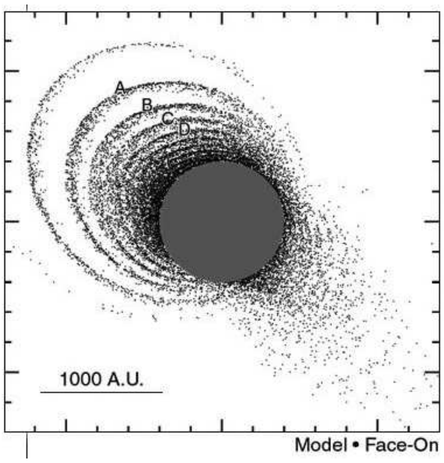

Figure 4: Larwood's simulation simulation of β Pictoris disc as shown in [27].

An alternative model is a fly-by by a perturbing star. With a 30° inclination of the perturbing star's trajectory to the circumstellar disc and a periastron of about size of the simulated disc, would generate the same large scale asymmetries, that is the difference in size and brightness between the wings, but also the inner warp. An interesting feature is also produced by simulating a fly-by, namely the ringing of the disc shown in Figure 4. [18] Comparing with the observation (Figure 5) opens the question what is seen and what is not. If there is some kind of ringing it does not seem to be a simple explanation of the spacing between the rings.

Stars perturbing β Pictoris in the past is possible to find in the Hipparcos catalogue. 18 stars have passed within 5 pc the last 1×10^6 years. The closest passing star is the K2III star HIP 27628 (~ 0.6 pc) and the dynamically

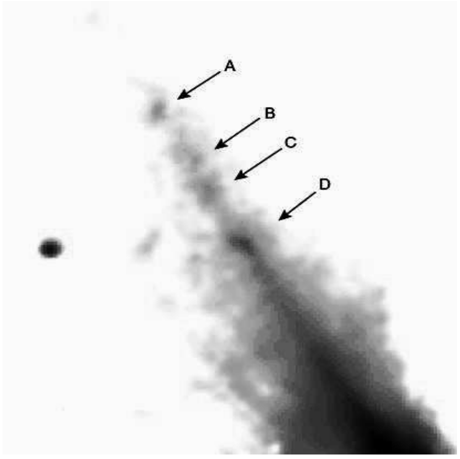

Figure 5: Observation of β Pictoris dust disc from [27]. To the left is a background star. Observing a ring structure in the β Pictoris dust disc is hard and there are no obvious equal spaceing between the enhancement of dust pointed out by the letters A,B,C,D.

most interesting star is the F7V star HIP 23693. But both of these encounters passed the star at too great distance to cause the kind of perturbation described above though. [16]

3 Dynamical Simulation

3.1 General equations

3.1.1 General assumptions

The simulation consists of a million collision-less test particles around a central star and perturbing star passing by. Both central star and perturber are considered as a point masses. The central star is labeled M_1 and the perturber M_2. The test particles are here represented by m. The distances $\vec{x}_0$, $\vec{x}_1$ and $\vec{x}_2$ are the distances from the origo O to the test particle, the central star and the perturber. $\vec{x}$ is the distance between central star and test particle. Examine Figure 6 for clarifications.

Considering only gravitation upon the test particle in inertial frame

$$\ddot{\vec{x}}_0 = -G\frac{M_1}{|\vec{x}|^3}\vec{x}_0 - G\frac{M_2}{|\vec{x}_0 - \vec{x}_2|^3}(\vec{x}_0 - \vec{x}_2) \tag{2}$$

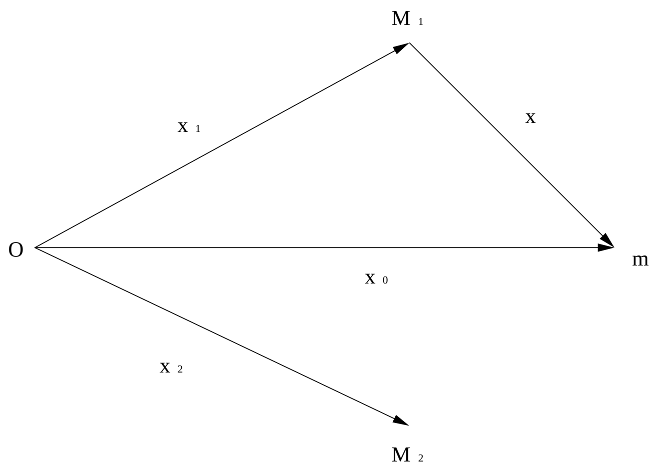

Figure 6: This figure explains in the nonaccellerated frame of reference the labeling of the distances and the masses.

Central star in inertial frame

$$\ddot{\vec{x}}_1 = -G\frac{M_2}{|\vec{x}_{12}|^3}(-\vec{x}_{12}) \tag{3}$$

Test particle in central star frame

$$\ddot{\vec{x}} = \ddot{\vec{x}}_0 - \ddot{\vec{x}}_1 = -G\frac{M_1}{|\vec{x}|^3}\vec{x} - G\frac{M_2}{|\vec{x}_0 - \vec{x}_2|^3}(\vec{x}_0 - \vec{x}_2) - G\frac{M_2}{|\vec{x}_{12}|^3}\vec{x}_{12} \tag{4}$$

In central star frame we can make following switch of variables

$$\vec{x}_1 \equiv \vec{0} \tag{5}$$

$$\vec{x}_0 \equiv \vec{x} \tag{6}$$

$$\vec{x}_{12} \equiv \vec{x}_2 \tag{7}$$

Applying this we get 8 there the length vectors between the masses are shown in Figure 7.

$$\ddot{\vec{x}} = -G\frac{M_1}{|\vec{x}|^3}\vec{x} - GM_2(\frac{\vec{x} - \vec{x}_2}{|\vec{x} - \vec{x}_2|^3} + \frac{\vec{x}_2}{|\vec{x}_2|^3}) \tag{8}$$

If test particles are small particles e.g. dust, radiation pressure will be of importance. β is defined as force due to radiation over gravitational force

$$\beta \equiv \frac{\vec{F}_{rad}}{\vec{F}_{grav}} \tag{9}$$

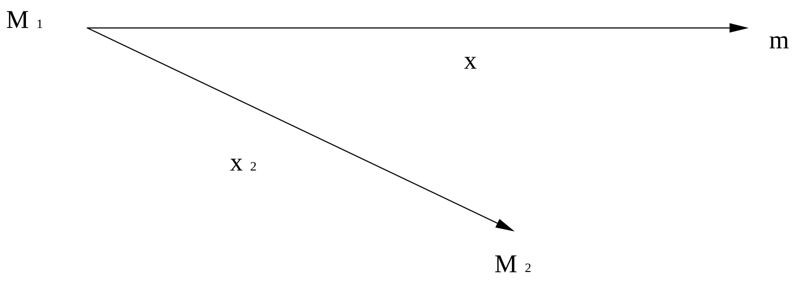

Figure 7: This figure explains in the accellerated frame of reference the labeling of the distances and the masses.

Knowing that the radiation force is repulsive and combining (8) with (9) results in

$$\ddot{\vec{x}} = -G\frac{M_1}{|\vec{x}|^3}\vec{x}(1-\beta) - GM_2(\frac{\vec{x}-\vec{x}_2}{|\vec{x}-\vec{x}_2|^3}(1-\beta) + \frac{\vec{x}_2}{|\vec{x}_2|^3}) \equiv \vec{f}(\vec{x}) \qquad (10)$$

3.1.2 Dynamics of the Perturber

The perturbing star's trajectory is calculated as following in the inertial frame

$$\ddot{\vec{x}}_2 = -G\frac{M_1}{|\vec{x}_{12}|^3}\vec{x}_{12} \qquad (11)$$

The perturber in the central star frame

$$\ddot{\vec{x}}_{12} = \ddot{\vec{x}}_2 - \ddot{\vec{x}}_1 = -G\frac{M_1}{|\vec{x}_{12}|^3}\vec{x}_{12} + G\frac{M_2}{|-\vec{x}_{12}|^3}(-\vec{x}_{12}) \qquad (12)$$

Applying variable exchange (5), (6) and (7) to equation above (12) we get the equation used in the simulation

$$\ddot{\vec{x}}_2 = -G\frac{\vec{x}_2}{|\vec{x}_2|^3}(M_1 + M_2) \qquad (13)$$

3.2 Physical setup for simulation

3.2.1 The Kalas-Larwood disc distribution

The distribution Kalas and Larwood used to produce their disc was with a surface number density $\Sigma(r) \propto r^{-3/2}$ and with a vertical density profile of $z(r) \propto r^{3/2}$. All particles are then set on an circular orbit around the central star. The disc abruptly ends at an outer radius of 535 AU.

To produce the disc from top-hat distributions some simple algebra is needed. Knowing that x_0 is sample from a top-hat distribution between 0 and 1 the corresponding sample from the Σ distribution is r_0

$$\int dN = \int \Sigma \, dA = \int_{rin}^{r_0} \Sigma(r) 2\pi r \, dr = \int_0^{x_0} dx \tag{14}$$

Solving for $r_0 = r_0(x_0)$ with parameters r_{in} r_{out} corresponding to inner and outer edge of disc it follows that

$$r_0(x_0) = (x_0(\sqrt{r_{out}} - \sqrt{r_{in}}) + \sqrt{r_{in}})^2 \tag{15}$$

The results from these calculations is shown in the Figure 8.

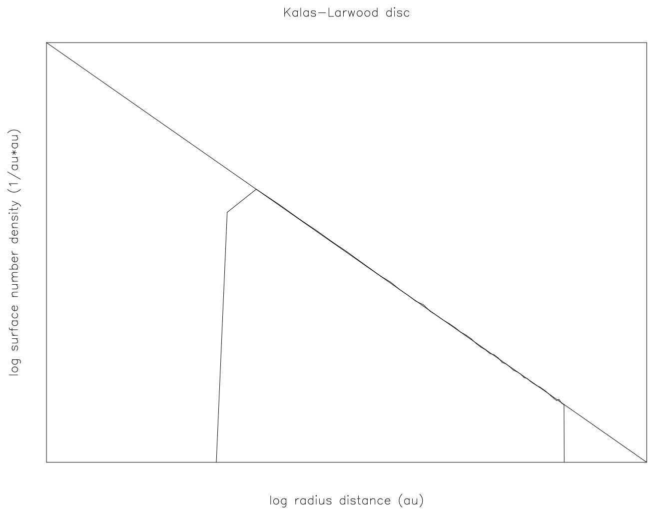

Figure 8: Reproducing the surface number density of the Kalas-Larwood disc from [18]. Both axis are logarithmic and the straight line show the desired $r^{-3/2}$ power law of the distribution.

There are problems with the Kalas-Larwood disc especially then radiation is switched on. As the particles from the radiation pressure get an increased energy and they therefore go from circular orbits to elliptic orbits. This will cause the disc to oscillate in an very specific manner. The radius of the gap in the disc around to the star starts to increase. The eccentricity of the orbit depends upon the size of the particle. The coupling between the radiation and the particle is for larger particles proportional to the inverse of its size. This will differentiate aphelion of the orbits of the particles and the oscillation will fade away if a sufficient number of periods is allowed.

Another interesting feature of Kalas-Larwood disc is the outer limit which causes an enhancement of outer most ring after the perturbation.

3.2.2 The stable disc distribution

To achieve a non-oscillating disc with no or at least an fuzzy outer limit, the particles were set on elliptical orbits with eccentricity e according to their β, which is derived by energy conservation and balancing forces. If a particle is orbiting a non-radiating object on a circular orbit gravity balance the centrifugal force.

$$\frac{GMm}{r_0} = \frac{mv^2}{r_0} \tag{16}$$

r_0 describe the pericentre distance and v the particles constant speed. If then radiation is switched on the particle will be at its pericentre with an increased amount of energy.

$$E_{total} = -G\frac{Mm}{r}(1-\beta) + \frac{mv^2}{r} = -G\frac{Mm}{2a}(1-\beta) \tag{17}$$

The equations (16) and (17) give $\beta = \beta(r_0, a)$. There is a relation binding the semi-major axis a with eccentricity e and pericentre distance r_0.

$$a(1-e) = r_0 \tag{18}$$

Using these three equations together (16), (17) and (18) it follow that

$$e = \frac{\beta}{1-\beta} \tag{19}$$

Kepler's equation was used to find the angle f from the pericentre to particles position on its orbit.

$$nt = f - e\sin(f) \tag{20}$$

The semi-major axis a is found from the periastron distance q which is picked from a distribution which is to mimic the number surface density $\Sigma(r)$ from Kalas-Larwood's disc.

$$a = \frac{q}{1-e} \tag{21}$$

To find a distribution which fits perfect is however difficult but by testing following (Figure 9) result is achieved there the straight line corresponds to the preferred theoretical $\Sigma(r) \propto r^{-3/2}$ distribution.

The distance from the central star to particle follows from

$$r = \frac{a(1-e^2)}{1+e\cos(f)} \tag{22}$$

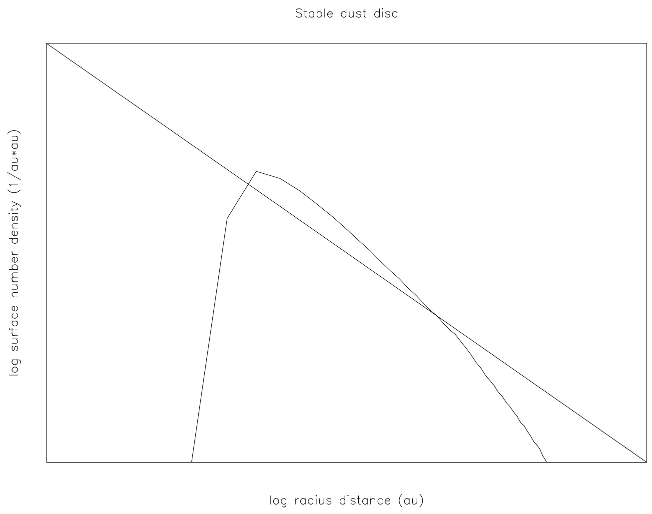

Figure 9: Calculating the surface number density of stable disc distribution this result is obtained. Both axis are logarithmic and the straight line show the desired $r^{-3/2}$ power law of the distribution.

Due to energy and angular momentum conservation the velocity in the plane of the trajectory is

$$v_\theta = \frac{\sqrt{a(1-e^2)}}{r} \tag{23}$$

$$v_r = \sqrt{\frac{2}{r} - \frac{1}{a} - \frac{a(1-e^2)}{r^2}} \tag{24}$$

If radiation pressure is accounted for it follows from (9) that equation (23) and (24) are modified by a factor

$$\sqrt{1-\beta} \tag{25}$$

To achieve fully 6 degrees of freedom in position and velocity the orbit is rotated by angle ω, inclined by an angle I and rotated once more by an angle Ω.

3.2.3 Initial condition of the Perturber

In the case of a parabolic trajectory the initial condition of the perturber are given on the form of the pericentre distance q and the initial distance of the perturber r_0. From geometry, position and velocity in plane of the conic section is as follow

$$x(|\vec{r_0}|, q) = 2q\sqrt{\frac{r_0}{q} - 1} \tag{26}$$

$$y(|\vec{r_0}|, q) = -r_0(1 - \frac{2q}{r_0}) \tag{27}$$

$$v_x(|\vec{r_0}|, q) = -\frac{y\sqrt{2q}}{x^2} - \frac{y^2}{2} - \sqrt{(\frac{y\sqrt{2q}}{x^2} + \frac{y^2}{2})^2 - \frac{4q - 2x^2}{r_0(x^2 + y^2)}} \tag{28}$$

$$v_y(|\vec{r_0}|, q) = \sqrt{\frac{2}{r_0} - v_x^2} \tag{29}$$

In the case of a hyperbolic trajectory the initial condition of the perturber is set by speed of perturber at infinity $|\vec{v}_\infty|$, pericentre distance q and the initial distance between the two stars r_0. Defining accretion radius r_a

$$r_a \equiv \frac{2G(M_1 + M_2)}{|\vec{v}_\infty|^2} \tag{30}$$

Using this definition, the geometry and the conservation of energy and angular momentum the position and velocity vector follows

$$y(|\vec{r_0}|, q, |\vec{v}_\infty|) = q\sqrt{1 + \frac{r_a}{q}} \tag{31}$$

$$x(|\vec{r_0}|, q, |\vec{v}_\infty|) = \sqrt{r_0^2 - q^2(1 + \frac{r_a}{q})} \tag{32}$$

$$v_r(|\vec{r_0}|, q, |\vec{v}_\infty|) = -|\vec{v}_\infty|\sqrt{1 + \frac{r_a}{r_0} - \frac{q^2}{r_0^2} - \frac{qr_a}{r_0^2}} \tag{33}$$

$$v_\phi(|\vec{r_0}|, q, |\vec{v}_\infty|) = \frac{q|\vec{v}_\infty|}{r_0}\sqrt{1 + \frac{r_a}{q}} \tag{34}$$

By using the following equation (from [6] on page 421) the angel Ψ needed to rotate the trajectory so that the it will be symmetrical around y-axis (Figure 10) is obtained.

$$\tan\Psi = -\frac{2b}{r_a} \tag{35}$$

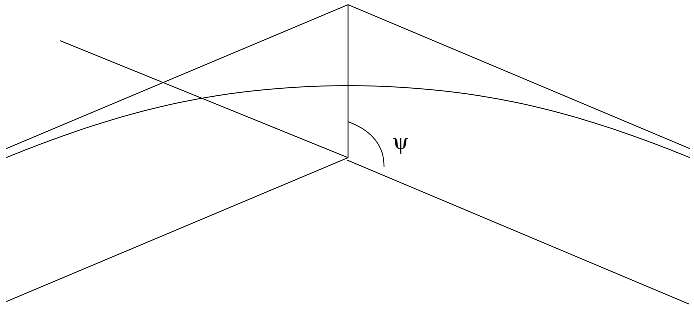

Figure 10: Angle of rotation to obtain the pericentre at the crossing of y-axis.

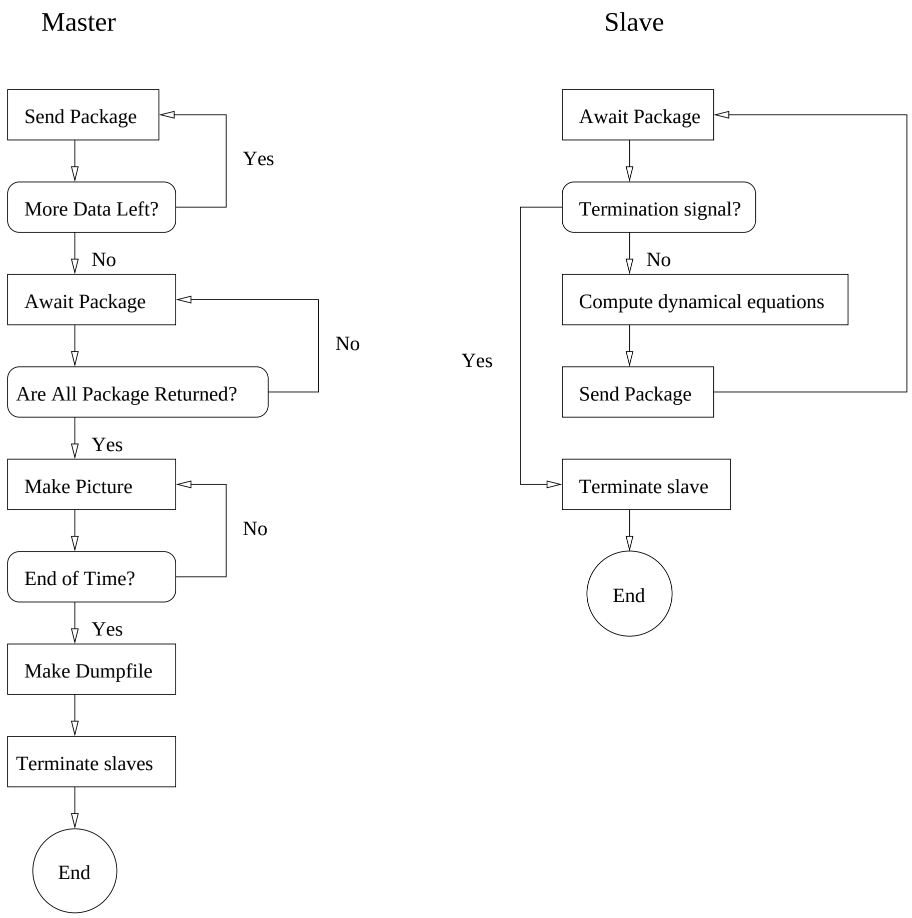

Figure 11: The program structure consists of two separate codes interacting to achive full usage of the Hydra clusters processors. See Section A.1 for more information about the cluster.

3.3 The Simulation

3.3.1 Program structure

The structure of the program running the simulation of the perturbed disc is a reflection of the hardware configuration and the problem. A Master code is run on the server art and a Slave code on each of the nodes. The following scheme (Figure 11) shows the interaction between the Master and the Slaves.

The workload is shifted from the Master to Slaves as the Master is run on a workstation also used for other purposes. The Master's task is to coordinate all actions of the Slaves and collect all information in order to produce an output which it stores on disc.

3.3.2 Numerical implementation

All number crunching is however done by the Slaves, which calculates the dynamical equations for the test particles using a Runge-Kutta routine of order 4. To solve $y' = f(x, y)$ with boundary condition $y(a) = y_a$ and step size h the routine used is as follow

$$k_1 = f(x_k, y_k) \tag{36}$$

$$k_2 = f(x_k + \frac{h}{2}, y_k + \frac{h}{2}k_1) \tag{37}$$

$$k_3 = f(x_k + \frac{h}{2}, y_k + \frac{h}{2}k_2) \tag{38}$$

$$k_4 = f(x_k + h, y_k + hk_3) \tag{39}$$

$$y_{k+1} = y_k + \frac{h}{6}(k_1 + 2k_2 + 2k_3 + k_4) \tag{40}$$

In order to solve equation (10) and (13) one must transforming the second order differential equation in to two equations of order one by defining $\vec{v} \equiv \dot{\vec{x}}$.

$$\dot{\vec{x}} = \vec{v} \tag{41}$$

$$\dot{\vec{v}} = \vec{f}(\vec{x}) \tag{42}$$

This makes a set of six equations per particle and iteration to solve. If all particles used the same step size all particles could form a vector of iteration with $6n$ rows. For at least two reasons it would be very inefficient to compute all particles with the same step size. First of all the particles are on very different orbital radii from the central star and even if they were constant in time, which they are not in the case of elliptic orbits, the particles would need different time steps. And second as the perturbing star comes close to the central star orbits change in dramatical ways which of course need greater accuracy.

Therefore each particle is given an individual step size which is controlled by a error check routine through out the simulation. The idea of this error control can be illustrated by Figure 12 there dx is the test particles step length in space and r is its distance from the closest star, here marked max. This fraction dx/r should be in a predefined interval of tolerance and if not the routine changes the time step so that it is.

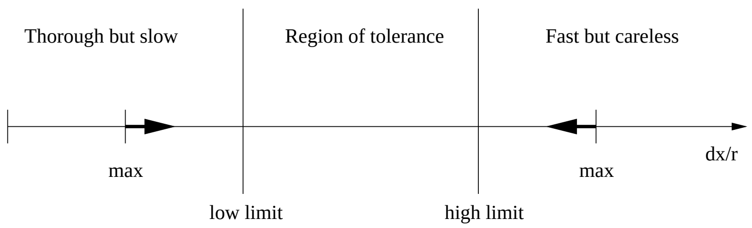

Figure 12: The calculation can either be thorough and slow or careless and fast, this implies that the user selects the region of tolerance to obtain the right balance between speed and accuracy.

One problem with the adaptable time step is that the star's positions must be computed for each step size of each and every one of the test particles. This problem is solved by precomputing a table of all possible step sizes for the stars before all the test particles computed using this table of positions. This has one draw back namely that there has to be a smallest step size, mean that the accuracy has one more predefined limit.

3.3.3 Accuracy

There are three simulations to examine, first the case with the perturber on a parabolic trajectory and the disc of Kalas-Larwood type. Second, the case of the perturber on a parabolic trajectory and a stable dust disc. Last, the case of the perturber on a elliptic orbit and a disc of Kalas-Larwood type.

trajectory	accuracy	step size
parabolic	0.5	0.005
dust	0.5	0.005
elliptic	0.125	0.0625

accuracy	0.125	0.0625	0.5
step size	0.25	0.125	0.005
mean energy difference	10^{-7}	10^{-8}	10^{-8}
mean square energy difference	10^{-7}	10^{-8}	10^{-7}
max energy difference	10^{-6}	10^{-7}	10^{-6}
massive body energy difference	10^{-12}	10^{-12}	10^{-10}

By combining the two tables a approximation of the accuracy can be obtained even if the actual energy changes from the respective simulations is not known. Important to have in mind is that the longer the simulation run the higher accuracy is needed to keep the additative errors down to a minimum.

3.3.4 Program output and PGPLOT

The PGPLOT Graphics Subroutine Library [28] is used to produce the images of the program output through out the simulation. PGPLOT is written in Fortran 77 but is callable from both C and Fortran. Using Fortran 90 one must link another library to have Fortran 77 library back compatibility. The output from PGPLOT can be on a great number of different devices or formats. GIF (Graphics Interchange Format) is mainly used but for some images PS (Postscript) was used namely those that are found in this text. PGPLOT is not free software and it is copyrighted by California Institute of Technology but can be used freely.

4 Results

4.1 Probability of perturbation

4.1.1 The passage of a field star

One question which one must ask oneself is how usual is the type of encounter need to produces the asymmetries of the disc. The perturber's velocity is crucial and can not correspond to hyperbolic trajectories simply because the time for interaction is too short, the disc does not have time to react. This produces another problem because background stars of population I and II have velocities corresponding to hyperbolic trajectories, typically $v_\infty = 40$ km/s respectively $v_\infty = 10$ km/s.

As mentioned in the introduction 18 stars were found to have passed within 5 pc of β Pictoris the last 1×10^6 years. This is a low number compared to a theoretical value computed by

$$\frac{dN}{dt} = \nu < v > \int_0^d 2\pi b \, db \tag{43}$$

Under a period of $\Delta t = 1 \times 10^6$ years, a stellar number density $\nu = 0.1$ per pc, and a mean velocity $< v >= 10$ km/s means that a $\frac{dN}{dt}\Delta t = 80$ stars will pass within a distance $d = 5$ pc of β Pictoris.

But to create a ring structure in the β Pictoris disc one must understand that, first it will not last for a long time, but the spacing between the rings can only survive for a short time $\Delta t \leq 50000$ years. To be dynamically interesting it shall pass at a distance $d = 750 \pm 250$ AU and if the perturber shall have time to interact with the disc its speed must be less than $< v >=$ 1km/s. The perturbers trajectory must intersect the disc within a certain interval of angles, $45°$ out of $360°$. And if the large scale asymmetries such as size and brightness are to be fulfilled also a certain interval of inclinations $I = 30° \pm 10°$. All in all $\frac{dN}{dt}\Delta t \sim 10^{-3}$ which means it is possible but very unlikely.

4.1.2 A binary companion

However an alternative could be an loosely bound binary. But what are the probabilities for this? This Gaussian (equation 44) describes the probability distribution of the orbital periods for binary stars according to [11]

$$b(\log T) \propto e^{-\frac{(\log T - \overline{\log T})}{2\sigma^2_{\log T}}} \tag{44}$$

where $\overline{\log T} = 4.8$, $\sigma_{\log T} = 2.3$ and there T is in days. Hence the probability to that a binary star has a period T or longer is $1 - \mathtt{P}$

$$\mathtt{P} = \frac{\int_{-\infty}^{\log T} b(\log T)\, d(\log T)}{\int_{-\infty}^{\infty} b(\log T)\, d(\log T)} \tag{45}$$

By using Kepler's third law the period T can be derived from the semi-major axis a and vice versa.

$$T^2 = \frac{\pi^2}{2(M_1 + M_2)G} a^3 \tag{46}$$

As the table below shows long period binaries are not very usual. If we when assume that β Pictoris has a binary companion then the more tightly bound the perturbing binary star is the more should it influence the disc. However what kind of disc is produced by this and does it contain the typical warp of β Pictoris?

$T\,(yr)$	$a\,(AU)$	$1-\mathtt{P}$
234344	10000	0.086
50000	3570	0.142
25000	2249	0.173

4.2 Sharp edges and fuzzy edges

Figure 13 is the reproduction Kalas and Larwoods result. [18] A perturbing star has passed by the central star at a distance of 695 AU with an inclination of 30° to the plane of the disc on a parabolic trajectory. The disc abruptly ends at 535 AU. This snapshot shows the simulation 90000 years after pericentre.

As mentioned above by reproducing the simulation from [18] confirms that the ring structure shown appears after approximately $\sim$ 90000 years after the pericentre. The ring structure shows a slightly elliptical tendency with the central star in one of the focal points. There are many rings after each other with progressively larger semi-major axis. Toward the central star the rings mix with each other so that the features become so small that the resolution given by the number of simulated particles is not good enough.

The description of the observed warp described as the Butterfly asymmetry in Section 2.3 is hard to match with this kind of simulation seen in Figure 14, due to that inside a radius of 200 AU the disc is hardly moved by the perturbing star.

A very interesting feature also appearing as a result of the Kalas-Larwood disc's edge (as described in Section 3.2.1) is the ring of increased surface density at a radial distance around 200 AU shown as a little bump on the otherwise rather smooth graph of Figure 17.

4.3 Dust discs

However if the disc lacks the abrupt end and consists of dust sensitive to radiation on noncircular orbits (as described in Section 3.2.2) pressure the ring structure is no longer visible (Figure 15). Although there is an elongation of the disc in the same direction as in the case of the planetesimal disc (Figure 13). As a result it is indicated that dust reflecting the thermal radiation from the star couples weakly with the assumed underlaying planetesimals.

It is important to understand why the planetesimals do not collide with each other and produce dust after the encounter, as described in [18]. And it is simply because most of the area in the disc are in smaller particles, which means that collisions between larger bodies are extremely rare in comparison with dust to plantesimal collisions and dust to dust collisions. That is

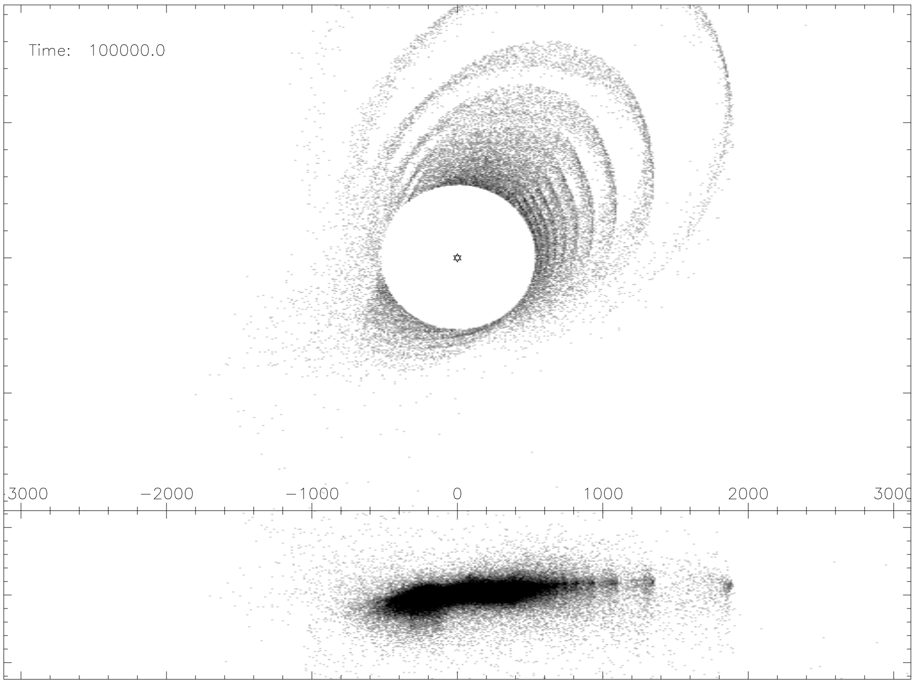

Figure 13: β Pictoris' disc 90000 years after the pericentre of a pertuber on a parabolic trajectory and 100000 years after initialization of the simulation. Scales are the same in the upper and the lower panel as well as along both x and y-axis and measured in AU.

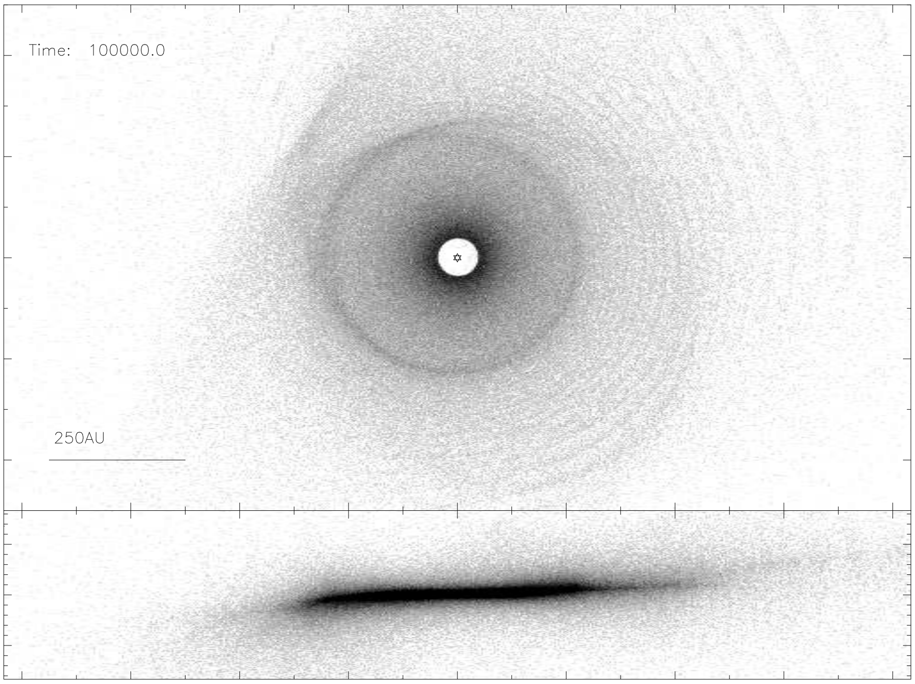

Figure 14: Close-up of β Pictoris' disc 90000 years after the encounter. Showning the nearly unperturbed inner parts of the disc.

structures in the planetesimal disc do not effect structures in dust disc.

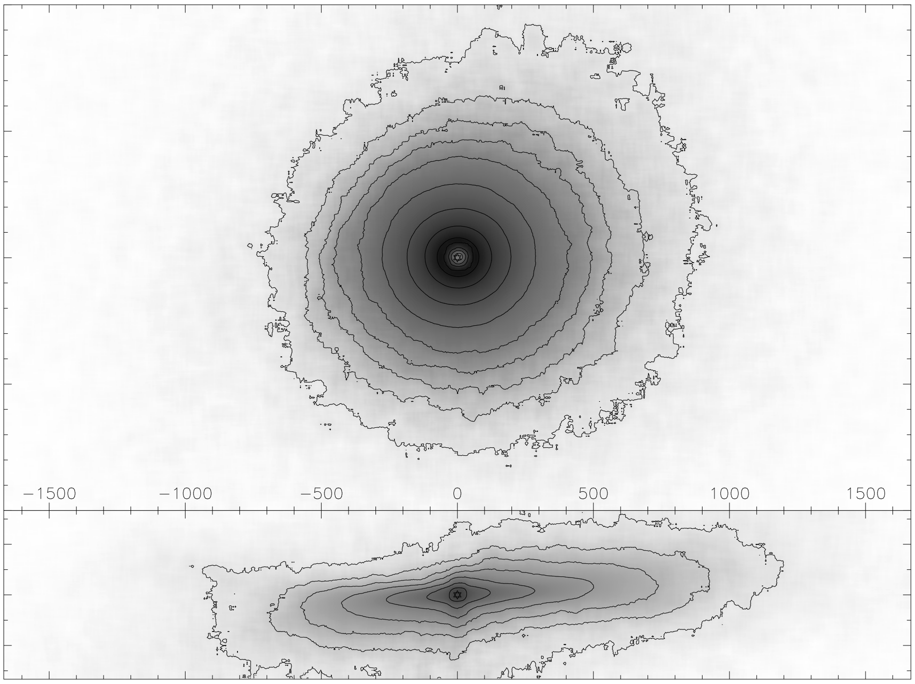

Figure 15: The simulated dust disc of β Pictoris shows no sign of a ring structure 90000 years after the encounter. Scales are the same in the upper and the lower panel as well as along both x and y-axis and measured in AU.

With a fuzzy edge in the initial state of the disc the 200 AU ring disappears, as seen in Figure 18. As the β Pictoris disc is known to have a smooth fuzzy edge this 200 AU ring would not appear in the observations even though a perturbation of the kind proposed by Kalas and Larwood [18], Kalas and Jewitt [17] and Kalas and Deltorn [16]. And as seen in Figure 15 the smaller rings of described ring structure leave no trace.

Comparing the HST/STIS observation in Figure 3 with the simulation in Figure 16 shows that the simulation have no or a very small warp.

By doing a binned profile of the planetesimal disc in the line of the outward progressing rings (Figure 19), that is at an angle of approximately 45° in picture reproduces to some extent the result of Kalas and Larwood. The figure shows the logarithm of intensity of brightness to the radius vector of the disc. This generally declining graph clearly shows the second outermost ring as a great bump.

Repeating this in the case of dusty disc (Figure 20) there are no obvious rings in the smoothly declining graph only some noise in the outer part of

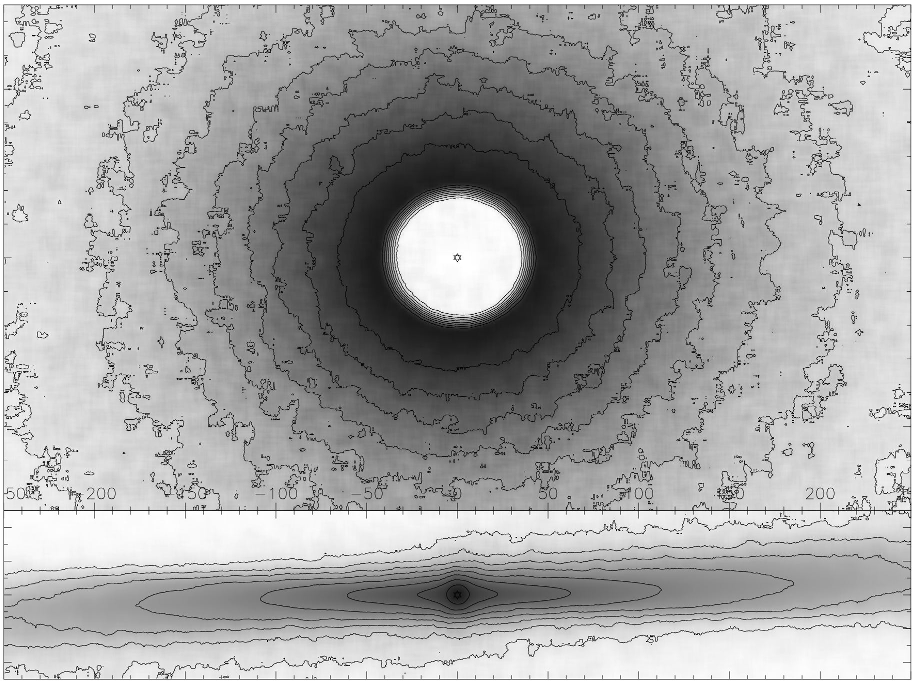

Figure 16: Close-up of the dust disc shows a that the disc tries to align with the perturbers trajectory, but the inner warping is negligible.

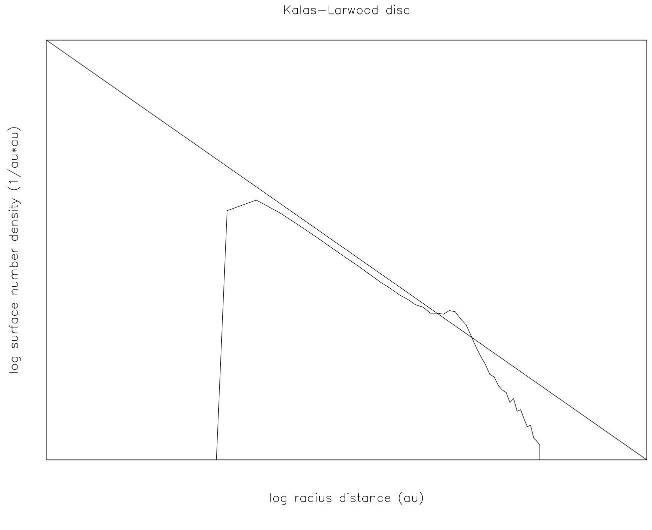

Figure 17: The surface number density of the Kalas-Larwood disc shows the 200 AU ring. The straight line through the picture represent the $r^{-3/2}$ power of preferred initial surface number density.

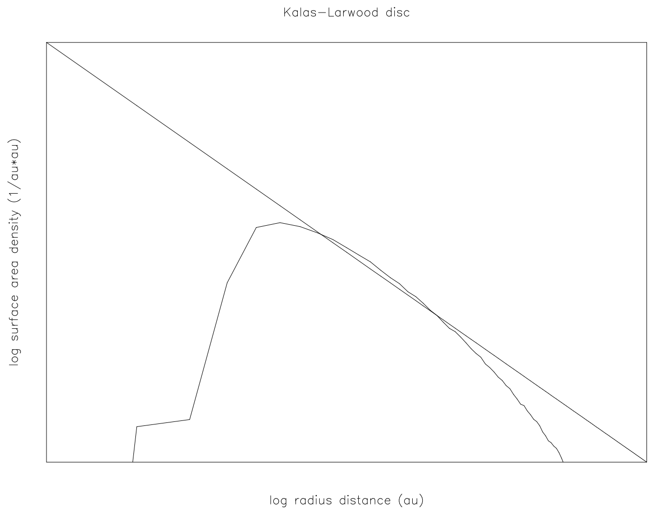

Figure 18: The surface number density of the stable dust disc is a smooth graph. The straight line through the picture represent the $r^{-3/2}$ power of preferred initial surface number density.

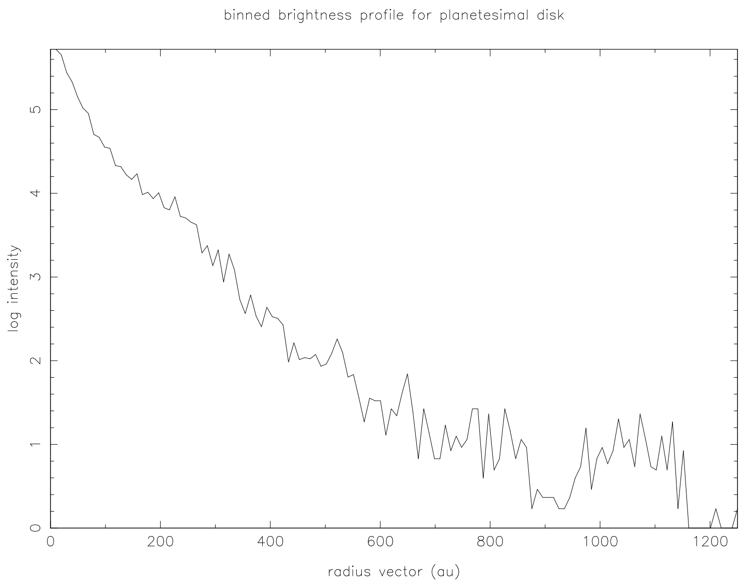

Figure 19: Binned profile of the planetesimal disc.

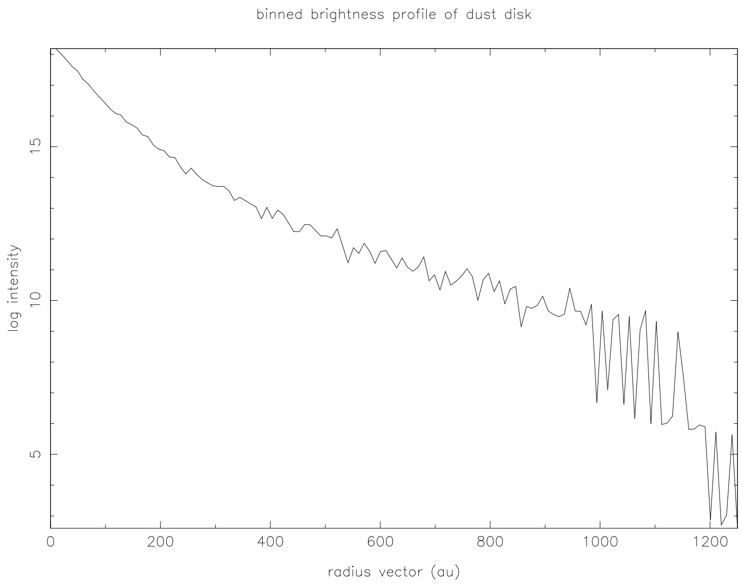

Figure 20: Binned profile of the stable dust disc.

the circumstellar disc ($r > 1150$ AU).

4.4 Repeated encounters

Simulating a binary star, that is a perturber on an elliptic orbit, what does a repeated encounter of this kind do with the ring and the over all structures of the disc? A disc of Kalas-Larwood type will be considered.

The first encounter (Figure 21) of the unperturbed disc produces a disc very much like the disc perturbed by an parabolic trajectory encounter, though the rings are somewhat more elliptic.

The rings disappear after the second encounter as seen in Figure 22, because the perturber rips the existing features apart and new weaker rings mix with the remains. And after a third encounter (Figure 23) there is definitely no ring structure to see in the simulation and a even though structure may exist but not be visible because of resolution they would not be observable with todays accuracy. Even the most likely not existing strongly pronounced 200 AU ring is somewhat washed away in the second encounter. For comparison see Figure 24, Figure 25 and Figure 26. Also notice that the disc's surface number density curve assumes a more rounded form like in the case of the dusty disc.

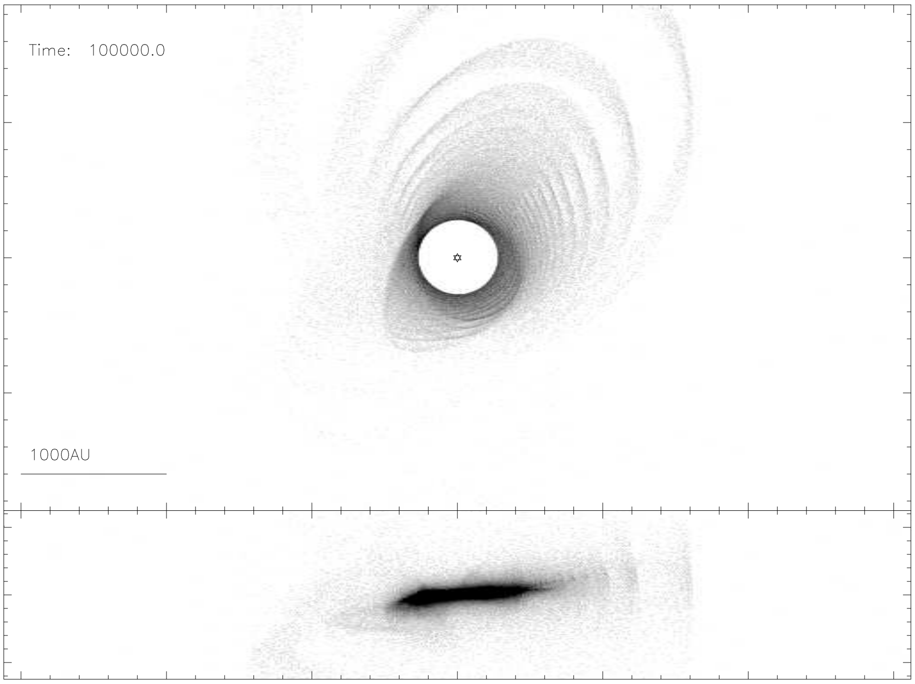

Figure 21: The β Pictoris planetesimal disc 90000 years after the first encounter on a elliptic orbit, with a mask covering the inner features of the disc.

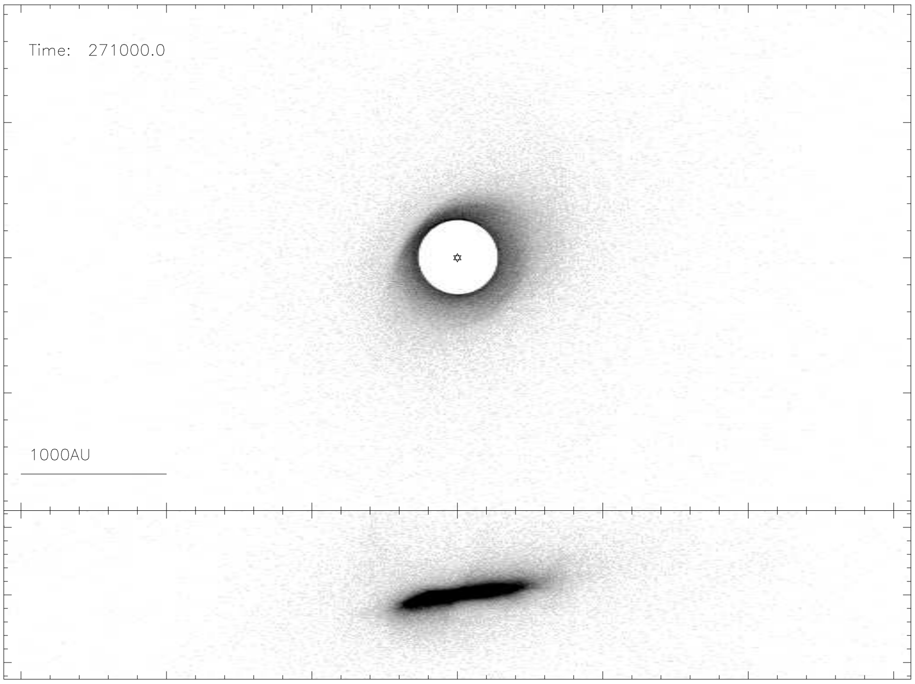

Figure 22: The β Pictoris planetesimal disc 90000 years after the second encounter on a elliptic orbit, with a mask covering the inner features of the disc.

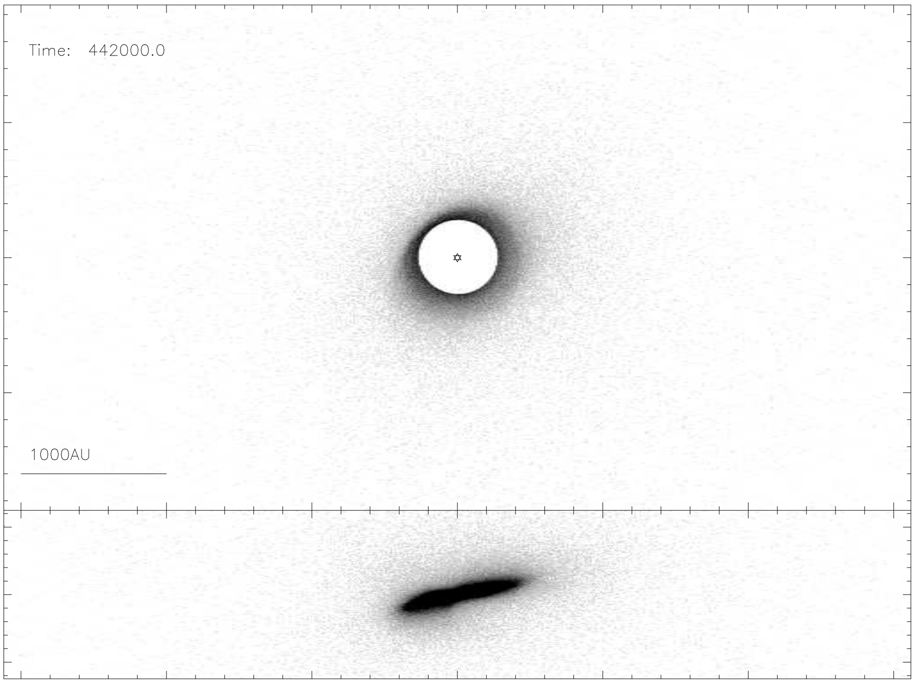

Figure 23: The β Pictoris planetesimal disc 90000 years after the third encounter on a elliptic orbit, with a mask covering the inner features of the disc.

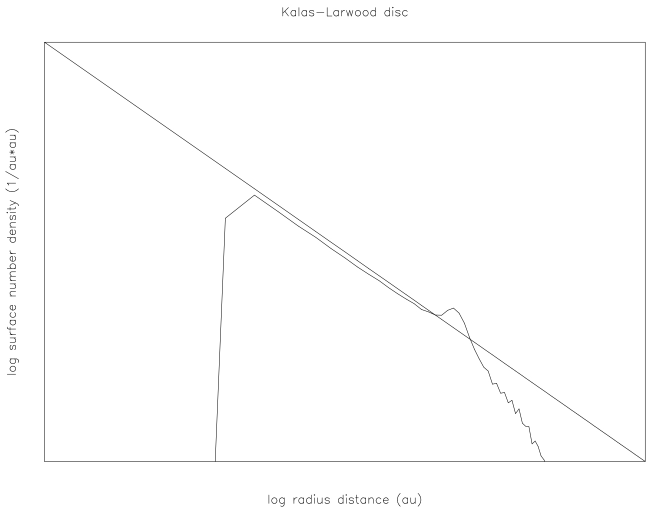

Figure 24: The surface number density of β Pictoris planetesimal disc 90000 years after the first encounter of its assumed binary star.

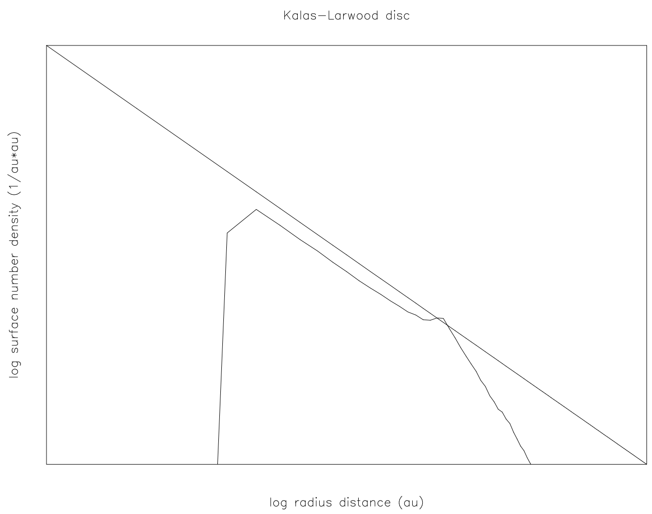

Figure 25: The surface number density of β Pictoris planetesimal disc 90000 years after the second encounter of its assumed binary star.

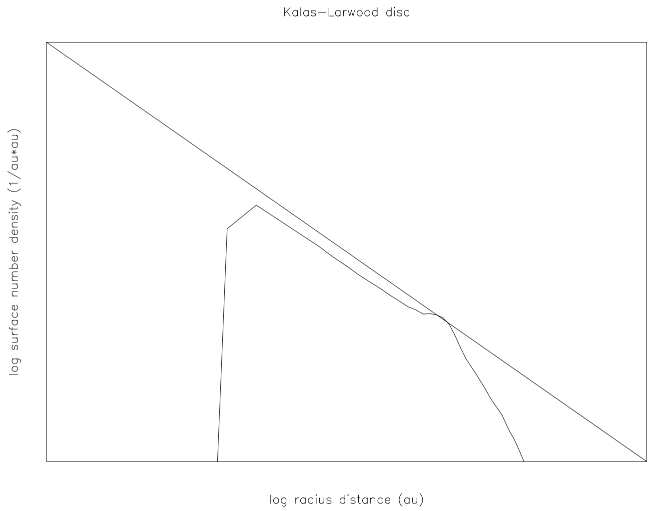

Figure 26: The surface number density of β Pictoris planetesimal disc 90000 years after the third encounter of its assumed binary star.

4.5 Hyperbolic encounter

In the case of a hyperbolic encounter the planetesimal disc differs little from the original unperturbed disc, both the size and the vertical structure remain weakly affected. Some rings can however be observed in this snapshot from a simulation. 30000 years after the encounter the ring features are at their most pronounced state. But already 90000 years after the encounter they are hard to see even at this, for a field star, relatively low velocity.

Therefore, the encounters of field stars with β Pictoris are not only very rare but also do not produce the desired structures, even in a disc of particles not affected by radiation pressure, which preserves such structures best.

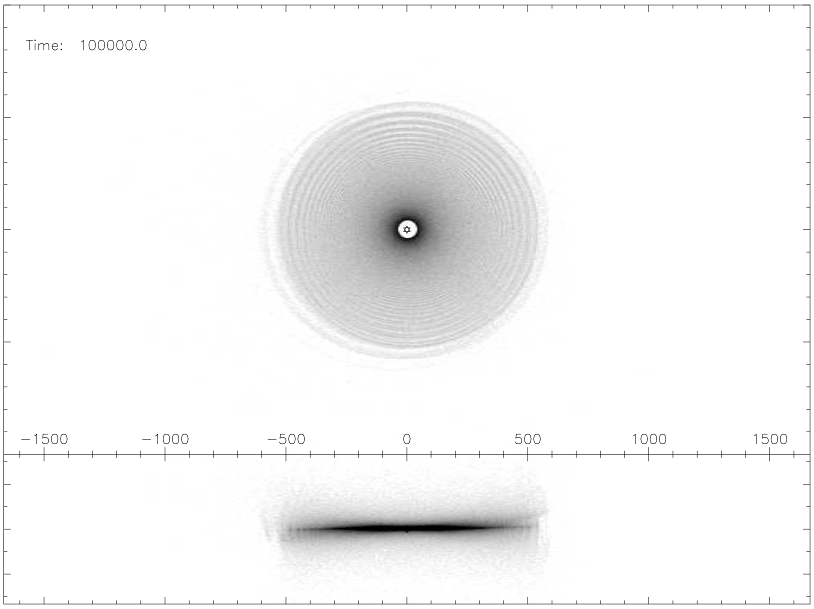

Figure 27: The β Pictoris' planetesimal disc perturbed by a star on a hyperbolic encounter with $v_\infty = 10$km/s.

5 Discussion

In conclusion, there are some problem with Kalas and Larwood's hypothesis of a perturbing star as an explanation of the asymmetries in β Pictoris dust disc especially the warp. The ringing affects the planetesimal disc of β Pictoris, but not the dust disc, which is in fact what is observed. The assumed ring structure has a weak theoretical explanation and no clear observational support.

The more likely alternative of n long period binary also disencourages the idea of a ring structure as each passage mixes the produced features from each encounter so that the clearly visible structure needed for a confirming observation vanishes.

The warp might be possible to recreate but it will demand very specific conditions for the perturber. And considering the small time interval this structure would remain in comparison with the likelihood of an encounter. It favours alternative explanations e.g. a planet inside the disc rather than an external object. The large scale asymmetries are however harder too exclude, but finding a singular explanation to the asymmetries is more appealing than a composite.

In the future it would be interesting to see more precisely how long the warped structure remains after an encounter to estimate the possibility of this being observed. A more exact comparison with the HST/STIS image would also be very nice. Also to create a routine to derive the exact condition needed to generate the observed warp, if this is at all possible with an ulterior object.

6 Conclusions

- It is in practice impossible to do the dynamical simulation with $\sim 10^6$ particles without parallel computing. Using MPI (Message Passing Interface) works well and makes the implementation easy.

- Kalas and Larwoods simulation was reproduced.

- Considered new physics as radiation pressure $\beta = \beta(s)$, where s is the size of a particle, together with a size distribution. This was cruical for the structure formation.

- Considered a more realistic disc with a fuzzy edge. This was important for the structure formation.

- Implemented a more detailed dust scattering code with a non-isotropic phase function $f = f(\theta)$. No large changes were seen.
- If the perturber is a field star there are several problems. First, the low probability of encounter. Second, it would be a hyperbolic encounter which due to the high speed would not have time to interact with the disc.
- Found that Kalas and Larwoods assumptions with no radiation pressure, a disc with a sharp edge and a parabolic encounter are maximizing the ring features but are inappropriate.
- A perturbing binary star blurs all edges and structures after a few passages even without the crucial radiation pressure.
- Therefore, the ring structure, if one, is unlikely due to an encounter.
- The case of binary catching field stars and throwing them at β Pictoris is estimated to have a low impact on the probability but needs a detailed evaluation.
- Some asymmetries can possibly be explained by a perturber but unlikely the inner warping. Maybe further investigations can throw some light on this.
- Kalas and Larwood's regular and periodic rings were not confirmed and must be seen as uncertain in the light of the present result.

7 Acknowledgments

First of all I would like to express my gratitude to my supervisor Docent Pawel Artymowicz who has inspired and helped me throughout this thesis, then the staff at Uppsala Observatory for encouraging my interest in astronomy and astrophysics, especially Dr. Nils Ryde.

And of course my friends and family who all made this possible.

A Appendix

In this section the concepts used in this thesis concerning parallel computing are covered. These are the ideas, the software and hardware used in the simulation.

A.1 The Hydra

Terminology is somewhat unsure but in the dawn of Beowulf clusters they were made out of low cost PCs running free software operating system Linux. In the taxonomy of parallel computers, Beowulf clusters fall somewhere between MPP (Massively Parallel Processors) and NOWs (Networks of Workstations) also known as COWs (Cluster of Workstations). Beowulf clusters tend to have slower connections between the nodes than MPPs but no need to compute under high work loads as on COWs.

The simulations were computed on the observatory's Hydra, which is a cluster of seven Sun Ultra Sparc Stations containing the Ultra Sparc II processor clocked at 333 MHz. The computers are connected via a 100 Mbps switch. The computers in the Hydra are sort of a high-end Beowulf machine with Art as a server. They are only used for computational purposes and can therefore be used at all hours and there is generally no need to accommodate the code to different workloads.

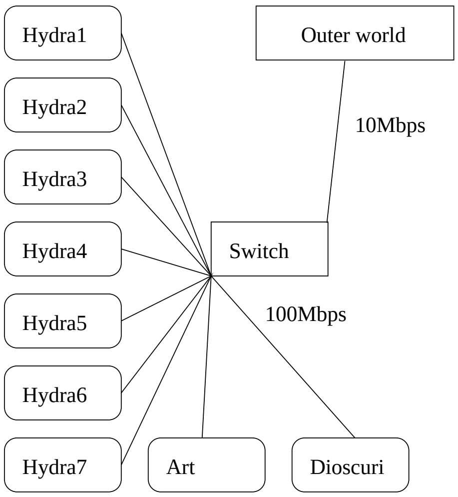

Figure 28: The Hydra Cluster

The operating system on all machines is the Sun Microsystems Operating System Solaris.

A.2 Fortran

All code for the simulation was written for Suns Fortran 90 compiler f90. There are several reasons for that. First of all Fortran is de facto standard in the world of astronomy and second the add on package PGplot is made for Fortran and easily linked in to the code.

Fortran 90 is preferred in comparison to Fortran 77 because of its ability to in a simple way allocate memory and ensure that the use of variables is not beyond the preselected ones. One big drawback with Fortran is the non-existing type checking, which under certain circumstances can cause trouble and make debugging more difficult than it has to be in other languages e.g. C++.

A.3 The MPI Standard

MPI stands for Message Passing Interface. MPI is standard for how to make an implementation of an interface used in message-passing programs. MPI is to be portable between different architectures and flexible for different ideas.

The MPI standard is developed by the the Message Passing Interface Forum (MPIF), with participation from over 40 organizations. They first met in November 1992 and work progressed till April 1994 and they discuss and define a set of library interface standards for message passing. The first version (1.0) was released on May 5, 1994. MPI-2 meetings began April, 1995 and and in April 25, 1997 all participants could agree on the document. Note that MPIF is not sanctioned or supported by any official standards organization. [30]

Included in the MPI standard version 1 is

- Point-to-point communication
- Collective operations
- Process groups
- Communication contexts
- Process topologies
- Bindings for Fortran 77 and C
- Environmental Management and inquiry
- Profiling interface

In the version 2 of the MPI standard are completely new types of functionality implemented, for example:

- dynamic processes
- one-sided communication
- parallel I/O
- Bindings for Fortran 90 and C++

A.4 Implementations

The implementation used for this simulation is MPICH [35] which has the

> "...design goal of combining portability with high performance."

The use is straight forward and easy to implement in fortran code. By compiling the program using the special command mpif90 the whole API of MPI become available.

LAM (Local Area Multicomputer) is another non-commercial and free implementation of the MPI standard and it completely supports MPI-1 compilance besides some aspects of MPI_Cancel. It also implements many of the MPI-2 commands. There are currently two versions of LAM v6.3.2 and v6.4-a3.

The later version of LAM has a feature called Interoperable Message Passing Interface (IMPI) which is a standardized protocol that enables different MPI implementations to communicate with each other. That makes it possible to use hardware specific implementations of MPI communicating with each other. This make it possible get the greatest performance from each of the integrated parts of whole system. [31]

Noteworthy in the commercial segment of MPI implementations are Suns MPI implementation which have a nearly complete MPI-2 compilance.

A.5 Performance comparison

A rather thorough test between the LAM 6.0 and MPICH 1.0.12 has been done. Mostly LAM has a better performance than MPICH but for very short segments of data there under some test MPICH beats LAM to the point. See [32]

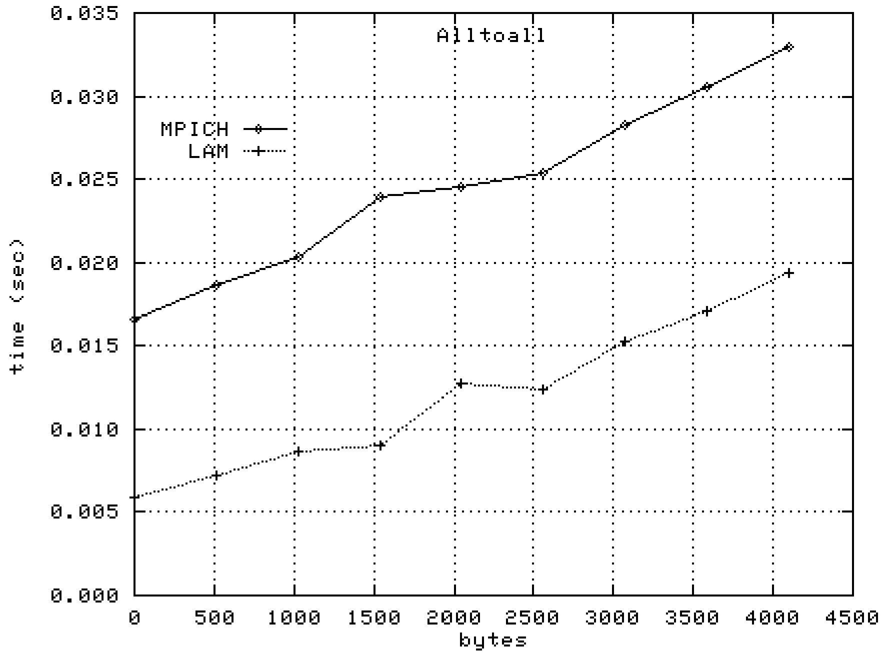

Figure 29: Preformance differences between LAM and MPICH

A.6 MPI Alternative

The main alternative to MPI is PVM (Parallel Virtual Machine) which is a similar kind of concept. It is created and maintained by Oak Ridge National Lab. It is not an open standard in the same sense as MPI and many people object to using it therefore. [29]

A.7 Comparing MPI and PVM

More work is being put down into MPI implementations, while PVM is developed by a single team, implying that MPI implementations are more up to date than PVM. [12]

There are many reasons to use MPI here are some: MPI has more than one freely available, quality implementation. That means that the choice of development tools is not coupled to the programming interface. MPI has full asynchronous communication, that means that the MPI standard allows the user to send and receive data at the same time. MPI efficiently manages message buffers by sending and receiving directly from the user data structures not by buffers within the communication library and therefore buffering may, in some cases, be totally avoided. A program written for MPI is completely portable, it is to recompile and run on any implementation. With virtual topologies and efficient buffer management a program will run well on just any hardware setup. MPI is formally specified through a standard and implementations have to live up to this very specific semantics. And features of MPI were derived in consensus by an open forum. And can only be changed under the same conditions. [33]

As PVM contains the ability to spawn processes, which the MPI standard lacks because it is primarily intended for data-parallel problems it does not have the flexibility of PVM achieved by the dynamic process spawning. But the MPI standards collective operations and asynchronous message passing capabilities are much more sophisticated and configurable than those in PVM. [34]

On the other hand it PVM is said to be more easily used and more adaptable to heterogeneous environments. The PVM demon also gives the user an additional help in debugging programs.

References

[1] Artymowicz, P., et al, *The Structure of the β Pictoris Circumstellar Disk From Combined IRAS and Cronographic Observation*, 1988, Preprint Series No. 294

[2] Artymowicz, P., et al, *Vega-Type Systems* 1996, Preprint No. 66

[3] Artymowicz, P., *Beta Pictoris: An Early Solar System?*, Annu. Rev. Earth Planet. Sci. 1997. 25:175-219

[4] Artymowicz, P. *Planet Formation and Disk Evolution* 2000, Proceedungs of the Conference 'Darwin and Astronomy - The Infrared Space Interferometer'

[5] Artymowicz, P., *Beta Pictoris and other Solar System*, Space Science Reviews 92: 69-86, 2000

[6] Binney, J., and S. Tremaine, *Galactic Dynamics,* 1987, Princeton

[7] Brandeker, A. *Rotation of β Pictoris disk*, 2001, Private communication at Stockholms Observatorium

[8] Cassen, P., and A. Moosman, *On the formation of protostellar disks* Icarus, 1982

[9] Cowley, C. R., *An Introduction to Cosmochemestry*, 1995, Cambridge Univerity Press, Cambridge Great Britain

[10] Dent, W. R. F., et al *Models of the dust structures around Vega-excess stars*, 2000, Mon. Not. R. Astron. Soc. 314, 702-712

[11] Duquennoy, A., and M. Mayor *Multiplicity among solar-type stars in the solar neighbourhood* 1991, Astronomy and Astrophysics 248, 485-524

[12] Geist, G. A., et al, *PVM and MPI: a Comparison of Features* 1996

[13] Gray, R. O., *A Digital Spectral Classification Atlas*, http://nedwww.ipac.caltech.edu/level5/Gray/Gray_contents.html

[14] Heap, S. R., et al, *STIS Coronagraphic Observations of β Pictoris* 1999, Astrophys. J.

[15] Jewitt, D. C., and J. X. Luu, *Physical Nature of the Kuiper belt* in *Protostars and Planets IV* 2000

[16] Kalas, P., and J.M. Deltorn, *Stellar Encounters with the β Pictoris Planetesimal System* 2001, astro-ph/0101364

[17] Kalas, P., and D. Jewitt, *Asymmetries in the Beta Pictoris Dust Disk*, 1995, The Astronomical Journal, Volume 110, Number 2, 794-805

[18] Kalas, P., and J. Larwood, *Rings in the planestesimal disk of β Pictoris*, 2000, The Astrophysical Journal, 530, L133

[19] Kant, I., *Allemeine Naturgeschichte und Theories des Himmels* (translation by W. Hashe), 1755, New York, Greenwood Publications, 1968

[20] Kaufmann, W., and A. Freedmann, *Universe Fifth Edition* 1998, New York

[21] Lin, D., *The Nebular Origin of The Solar System*, in *The Solar System: Observation and Interpretations*, (M. G. Kivelson, ed.) 1986, New Jersey

[22] Malfait, K., *The properties and evolution of the dusty disks surrounding Herbig Ae/Be stars*, 1999, http://www.ster.kuleuven.ac.be/˜koenm/thesis/thesis.html

[23] Schwarzschild, M., *Strucure and Evolution of the Stars*, 1958, N.J.

[24] Strom SE., S. Edward, and MF. Skrutskie, *Evolutionary time scales for circumstellar disks assocated with intermediate- and solar type stars*, in *Protostar and Planets III* 1993

[25] Takeuchi, T., and P. Artymowicz, *Dust Migration and Morphology in Optically Thin Cicumstellar Gas Disks*, 2001, Submitted to Astrophysical Journal

[26] Vidal-Madjar, A., et al, *β Pictoris, a young planetary system? A review*, 1997, Planet. Space Sci., Vol 46, No. 6/7 pp. 629-648

[27] Villard, R., and P. Kalas, *Beta Pictoris Disk Hides Giant Elliptical Ring System*, Hubble Space Telescope NEWS, PRESS RELEASE NO.: STScI-PR00-02

[28] http://www.astro.caltech.edu/˜tjp/pgplot/

[29] http://www.epm.ornl.gov/pvm/pvm_home.html

[30] http://www.mpi-forum.org/

[31] http://www.mpi.nd.edu/lam/

[32] http://www.mpi.nd.edu/lam/papers/perf/

[33] http://www.mpi.nd.edu/lam/mpi/mpi_top10.php3

[34] http://www.ncsa.uiuc.edu/SCD/Hardware/CommonDoc/MessPass/

[35] http://www-unix.mcs.anl.gov/mpi/mpich/